Inorganic Chemistry

ARTICLE

pubs.acs.org/IC

On the Nature of the Multiple Ground States of the MMX Mixed-Valence Chain Compound, $[Pt^{II/III}_2(n\text{-}PenCS_2)_4I]_\infty$

Minoru Mitsumi,*[,†] Takami Yamashita,[†] Yuko Aiga,[†] Koshiro Toriumi,*[,†] Hiroshi Kitagawa,[‡,∥] Tadaoki Mitani,[‡,⊥] and Mohamedally Kurmoo[§]

[†]Department of Material Science, Graduate School of Material Science, University of Hyogo, 3-2-1 Kouto, Kamigori-cho, Ako-gun, Hyogo 678-1297, Japan

[‡]Japan Advanced Institute of Science and Technology, Tatsunokuchi, Ishikawa 923-1292, Japan

[§]Laboratoire DECOMET, CNRS-UMR 7177, Université de Strasbourg, CS 90032, 4 rue Blaise Pascal, F-67081 Strasbourg, France

Supporting Information

ABSTRACT: We present a comprehensive study of the temperature dependence of the crystal structure using single-crystal X-ray diffraction and diffuse scattering, and electrical transport and magnetic properties as well as some optical properties at room temperature to elucidate the origin and the form of multiple ground states demonstrated in a previous study of the heat-capacity of the MMX chain compound, $[Pt^{II/III}_2(n\text{-}PenCS_2)_4I]_\infty$. The present results confirm the presence of the two phase transitions, one reversible of first order at 207 K and the other nonreversible monotropic at 324 K, separating the low temperature (LT), room temperature (RT), and high temperature (HT) phases. The unit cell displays a 3-fold periodicity of −Pt−Pt−I− in the RT and HT phases because of the structural disorder which is exhibited by the dithiocarboxylato groups and the *n*-pentyl groups belonging to the central diplatinum unit. In addition, for the HT-phase all the dimers show this disorder. This compound undergoes a metal−semiconductor transition at T_{M-S} = 235 K. The presence of diffuse streaks corresponding to 2-fold −Pt−Pt−I− periodicity in the HT and RT phases indicates dynamic valence ordering of the type —Pt^{2+}—Pt^{2+}—I^--Pt^{3+}-Pt^{3+}-I^-—or—Pt^{2+}–Pt^{3+}-I^--Pt^{3+}–Pt^{2+}—I^-—. For the LT-phase the diffuse scattering is condensed into clear Bragg diffraction peaks while keeping the 3-fold periodicity. This fact suggests further localization through dimerization of charges and spins confirming the diamagnetic state in the magnetic susceptibility and the low electrical conduction below 207 K. The present results are further discussed in relation to those of previous studies on the homologues, $[Pt^{II/III}_2(RCS_2)_4I]_\infty$, R = methyl, ethyl, *n*-propyl, and *n*-butyl.

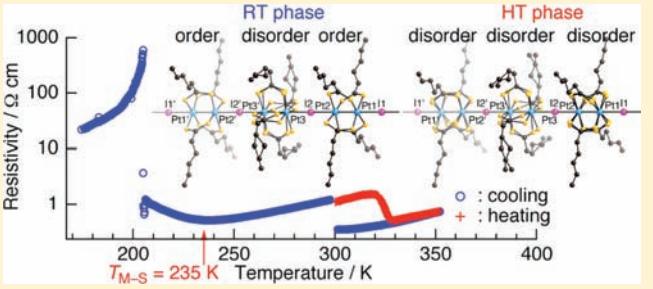

1. INTRODUCTION

Materials having one-dimensional structures based on molecular building blocks have been pivotal in the understanding of the chemistry and physics of conducting, magnetic, and optical properties for they are appealing to theoreticians because of the simplicity of structure and to chemists because of the ease of modification to achieve different variants via solution syntheses. Among the range of materials known the mixed-valence platinum chains have a very special place because they were the first to attract attention because of their variable intense colors and unusual metallic luster.[1,2] Also they were the first to be recognized to develop Peierls instability due to the pairing of unpaired electrons during lattice dimerization.[3] Between those containing a direct metal−metal chain, such as $K_2[Pt(CN)_4]Br_{0.3}$ (KCP(Br)),[3,4] and those having a metal−halogen−metal chain, such as the Wolffram's red family $[Pt^{II}(NH_2Et)_4Pt^{IV}(NH_2Et)_4Cl_2]Cl_4$ (known as MX chain),[5,6] lies the $(metal)_2$−halogen−$(metal)_2$ chain, where two families have been realized differing in the equatorial ligand, POP^{2-} = $H_2P_2O_5^{2-}$ or alkyl dithiocarboxylate.[7−18] They are labeled as MMX. In contrast to the MX compounds where the valences alternate with Pt^{2+} and Pt^{4+}, the MMX ones are formed from $(Pt^{2+})_2$ and $(Pt^{3+})_2X_2$ where the difference is still two electrons but for the latter the spin state of the Pt^{3+} is paramagnetic $S = 1/2$. This difference in electronic configurations and the presence of dimers, increase the number of possible ground states from two for MX to four for MMX as follows:

(a) averaged valence (AV) state :

$$-M^{2.5+}-M^{2.5+}-X^-M^{2.5+}-M^{2.5+}-X^-$$

(b) charge-polarization (CP) state :

$$—M^{2+}-M^{3+}\text{-}X^-—M^{2+}-M^{3+}\text{-}X^-—$$

(c) charge density wave (CDW) state :

$$—M^{2+}—M^{2+}—X^-\text{-}M^{3+}\text{-}M^{3+}\text{-}X^-$$

Received: December 8, 2010
Published: April 12, 2011

   dx.doi.org/10.1021/ic102461z | *Inorg. Chem.* 2011, 50, 4368–4377

Table 1. Details of the Crystal Chemistry and Transport Properties of the $[Pt_2(RCS_2)_4I]_\infty$ Series

R	methyl	ethyl	*n*-propyl	*n*-butyl	*n*-pentyl
space group in RT phase	*C*2/*c*	*C*2/*c*	*I*4/*m*	*I*4/*m*	*I*4/*m*
periodicity in LT phase		2[f]	6[i]	2[f]	6[k]
periodicity in RT phase	1[a,b]	1[a,g]	3[a,i]	3[a,f]	3[a,k]
periodicity in HT phase	1[a,c]		1[a,i]	1[a,k]	3[a,k]
LT−RT transition		∼180 K and ∼230 K[h]	209 K[j] higher-order	213.5 K[l] first-order	207.4 K[m] first-order
RT−HT transition	373.4 K[d] first-order		358.8 K[j] first-order	323.5 K[l] first-order	324 K[m] monotropic
metal-semiconductor transition	300 K[e]	205 K[g]	nonthermally activated type above 330 K[i]	325 K[f]	235 K[k]

[a] Diffuse streaks with the 2-fold repetition length of a −Pt−Pt−I− period were observed. [b] Reference 8a. [c] Reference 9c. [d] Reference 18a. [e] Reference 10. [f] Reference 12. [g] Reference 11. [h] Reference 18b. [i] Reference 13. [j] Reference 18c [k] This work. [l] Reference 18d. [m] Reference 18e.

(d) alternate charge-polarization (ACP) state :

$$—M^{2+}—M^{3+}\text{-}X^{-}\text{-}M^{3+}—M^{2+}—X^{-}—$$

The valence state, expressed as a $—M^{2+}—M^{3+}$-, represents an extreme case, which can be more accurately represented as $—M^{(2+\delta)+}—M^{(3-\delta)+}$- or $—M^{(2.5-\delta)+}—M^{(2.5+\delta)+}$- ($0 \le \delta \le 0.5$). The AV and CP states in which the periodicity of the one-dimensional (1-D) chain is −M−M−X− correspond to a metallic state with an effective half-filled conduction band mainly composed of M−M $d\sigma^*$−X p_z hybridized orbitals or to a Mott−Hubbard semiconducting state. In contrast, the periodicities of the 1-D chains in the CDW and ACP states are doubled. Except for AV, the valence-ordered states of the other three are expected to undergo lattice distortions because of valence alternation. These diverse electronic structures are expected to facilitate valence delocalization and enhance valence fluctuation in the mixed-valence state.

The aim for increasing the ratio of Pt to halogen in the chains was to increase the conductivity from semiconducting to metallic, and the first observation of metallic conductivity was made for $[Pt_2(MeCS_2)_4I]_\infty$ above 300 K.[10] To extend the limits, further development that continues was to replace the methyl group by longer chain alkyl groups which is expected to reduce transversal effects and increase the conductivity further. The results were positive. Furthermore, the elongation of the alkyl chains introduces increasing motional degrees of freedom in the system. Interplay between electronic degrees of freedom and molecular dynamics is also expected to cause a structural phase-transition accompanying an electronic and/or magnetic transition not observed for $[Pt_2(MeCS_2)_4I]_\infty$. Along this line, we have studied the series of MMX chain compounds, $[Pt_2(RCS_2)_4I]_\infty$ (R = Et,[11,12] *n*-Pr,[13] *n*-Bu[12]) and have investigated the relationship between crystal structures and solid-state properties. The key features of the results are given in Table 1.

With the elongation of the alkyl chains in ligands, the crystal structure at room temperature changes from the monoclinic *C*2/*c* in $[Pt_2(RCS_2)_4I]_\infty$ (R = Me,[8a] Et[11]) to the tetragonal *I*4/*m* in $[Pt_2(RCS_2)_4I]_\infty$ (R = *n*-Pr,[13] *n*-Bu[12]). The lattice periodicity along the 1-D chain direction of the latter two compounds is 3-fold of a −Pt−Pt−I− period, and this periodicity is associated with the structural disorders of the two PtS_4 planes and alkyl chains belonging to only the central diplatinum unit in the 3-fold periodic structure.[13,12] These two compounds undergo a first-order phase transition or higher-order phase transition at near 210 K and above room temperature with increasing motional degrees of freedom in the system. The unit cell dimension *c* along the 1-D chain direction of $[Pt_2(n\text{-}PrCS_2)_4I]_\infty$ changes to 1-fold periodicity in the HT phase while keeping the same space group, and the two PtS_4 planes of all the diplatinum units are disordered over two sites.[13] On the other hand, we have found from the crystal structure analyses that the lattice periodicity of $[Pt_2(RCS_2)_4I]_\infty$ (R = Et, *n*-Bu) along the 1-D chain direction changes to 2-fold periodicity in the LT and, from Pt−Pt and Pt−I bond distances, the valence-ordering state is assigned to the ACP state.[11,12]

A preliminary study of the crystal structure and heat capacity of $[Pt_2(n\text{-}PenCS_2)_4I]_\infty$ (**3**) having the next longer alkyl member, *n*-pentyl group, has been reported by some of us where it was found that there were two phase transitions at 207.4 and 324 K, where the former is of first-order and reversible but the latter is monotropic, that is, irreversible.[18e] To elucidate the different ground states, we have extended the previous work by studying the crystal chemistry by single-crystal X-ray diffraction and diffuse scattering, and electrical and magnetic properties as a function of temperature. Some optical measurements at room temperature are also reported. The unit cell of **3** displays a 3-fold periodicity of −Pt−Pt−I− in a ratio of two crystallographically independent dimer units being 2:1 in the RT and HT phases, because of the presence of mirror planes of the *I*4/*m* space group, and presents disorder of the two PtS_4 planes of the central Pt−Pt unit over two sites. In addition, for the HT-phase all the dimers show this disorder. This compound undergoes a metal−semiconductor transition at T_{M-S} = 235 K. The appearance of diffuse streaks with 2-fold −Pt−Pt−I− periodicity and their condensation into well-defined Bragg spots at low temperatures while keeping the 3-fold periodicity match very well with the metal−insulator (LT-RT) and the metal−metal (RT-HT) transitions observed in the transport properties and the paramagnetic to diamagnetic susceptibility. These observations gave clear definitions of the ground states in all three regimes. Furthermore, the crystal structure analysis of $[Pt_2(n\text{-}BuCS_2)_4I]_\infty$ (**4**) in the HT phase has also been carried out at 350 K to compare with that of **3** in the HT phase.

2. EXPERIMENTAL SECTION

Synthesis. Unless otherwise stated, all manipulations were performed at room temperature under argon atmosphere using standard vacuum line and Schlenk techniques. All solvents were dried using appropriate drying agents and freshly distilled under argon before use.[19]

dx.doi.org/10.1021/ic102461z |*Inorg. Chem.* 2011, 50, 4368–4377

Table 2. Crystal Data and Details of Structure Refinements for 3 and 4

compound	3 - RT phase	3 - HT phase	4 - HT phase
formula	$C_{24}H_{44}IPt_2S_8$	$C_{24}H_{44}IPt_2S_8$	$C_{20}H_{36}IPt_2S_8$
fw	1106.15	1106.15	1050.05
T, K	250	270	350
cryst size, mm^3	0.10 × 0.07 × 0.06	0.07 × 0.07 × 0.08	0.27 × 0.16 × 0.15
wavelength, Å	0.5633(1)	0.5633(1)	0.71069
crystal system	tetragonal	tetragonal	tetragonal
space group	$I4/m$	$I4/m$	$I4/m$
a, Å	14.2587(10)	14.2574(14)	13.6271 (15)
c, Å	25.8368(18)	25.8988(18)	8.6043 (13)
V, Å^3	5252.9(6)	5264.5(8)	1597.8 (3)
Z	6	6	2
D_c, g cm^{-3}	2.098	2.093	2.183
μ, mm^{-1}	4.822	4.811	10.244
$F(000)$	3 150	3 150	986
θ_{min}, θ_{max}, deg	1.29, 21.45	1.29, 21.45	1.000, 29.96
no. of total reflections	21 401	17 093	2549
no. of unique reflections	3 095	3 098	1231
R_{int}	0.0300	0.0294	0.0490
no. of observed $[I > 2\sigma(I)]$	1 356	1 393	1061
$R1$, $wR2$ $[I > 2\sigma(I)]$	0.0595, 0.2456	0.0741, 0.3309	0.0244, 0.0550
$R1$, $wR2$ (all data)	0.1007, 0.2568	0.1100, 0.3442	0.0304, 0.0572
GOF	1.151	1.114	1.100
max, min $\Delta\rho$, e Å^{-3}	1.258/−1.280	1.334/−1.334	0.443/−1.795

Dithiohexanoic acid, n-PenCS$_2$H,[20] and $[Pt_2(n\text{-BuCS}_2)_4I]_\infty$ **(4)**[12] were prepared according to published procedures.

$[Pt_2(n\text{-PenCS}_2)_4]$ (1). To a suspension of $PtCl_2$ (1.438 g, 5.406 mmol) in 135 mL of toluene, dithiohexanoic acid (3.201 g, 21.59 mmol) in 25 mL of toluene was added under an argon atmosphere. The mixture was refluxed for 6 h with stirring during which the solution turned dark red. After cooling, the toluene was evaporated to almost dryness using a rotary evaporator and to the residue n-hexane was added. The resulting dark red needle crystals were filtered, washed with n-hexane. The crude product (2.144 g) was dissolved in 10 mL of toluene at 50 °C and then the solution filtered. 70 mL of n-hexane was added to the filtrate and allowed to stand for 1 h. The dark red needle crystals with copper luster separated from the solution. These were collected by suction filtration and then washed with n-hexane (2.028 g, 77%). Anal. Calcd. for $C_{24}H_{44}Pt_2S_8$: C, 29.44; H, 4.53. Found: C, 29.37; H, 4.47%.

$[Pt_2(n\text{-PenCS}_2)_4I_2]$ (2). **1** (791 mg, 808 mmol) was dissolved in 40 mL solution of iodine in toluene (249 mg, 981 mmol), and the reaction mixture was heated at 60 °C for 45 min while stirring. After cooling, the toluene was evaporated to about 5 mL, and then 60 mL of n-hexane was slowly added. The resulting deep purple crystals were collected by suction filtration and washed with n-hexane (930 mg, 93%). Anal. Calcd. for $C_{24}H_{44}I_2Pt_2S_8$: C, 23.38; H, 3.60. Found: C, 23.30; H, 3.55%.

$[Pt_2(n\text{-PenCS}_2)_4I]_\infty$ (3). **1** (59 mg, 60 mmol) and **2** (63 mg, 51 mmol) were dissolved in 2 mL of toluene at 65 °C and 29 mL of n-hexane was added to the solution. The solution was heated at 65 °C for 1 h while stirring and then slowly cooled to 0 °C. The resulting black needle crystals were collected by suction filtration and washed with acetone to dissolve the excess of **2** deposited with **3** (91 mg, 81% yield based on **2**). Anal. Calcd. for $C_{24}H_{44}IPt_2S_8$: C, 26.06; H, 4.01. Found: C, 25.97; H, 3.96%.

UV−Visible−Near-IR and IR spectroscopy. UV−Visible−Near-IR spectra of the complexes as KI or KBr pressed disks were recorded on a Hitachi U-3500 spectrophotometer equipped with a 60 mm ϕ integrating-sphere apparatus. IR spectra were recorded as KI or KBr pressed disks on a Horiba FT-200 spectrophotometer.

X-ray Crystal Structure Analyses. A summary of the crystallographic data and intensity data collection for **3** and **4** is given in Table 2. Crystallographic information files (CIF) for all data sets are provided in the Supporting Information.

$[Pt_2(n\text{-PenCS}_2)_4I]_\infty$ (3) in the RT and Supercooled HT Phases and Diffraction Experiments. X-ray diffraction experiments of **3** were performed using synchrotron radiation (22.011(5) keV, λ = 0.5633(1) Å) and a Rigaku large cylindrical image-plate camera equipped with a Rigaku variable temperature apparatus based on a cold nitrogen gas stream method at the BL02B1 beamline of SPring-8. Single crystals were mounted on glass fibers with epoxy resin. To reveal the origin of the monotropic nature of the RT−HT phase transition, the crystal structure analysis of the supercooled HT phase was carried out at 270 K using a crystal once heated to 350 K.

Cell refinements, indexing, peak integrations, and scaling of the diffraction data sets were carried out using the program RAPID AUTO. Lorentz, polarization, and a numerical absorption correction were applied to the intensity data.

$[Pt_2(n\text{-BuCS}_2)_4I]_\infty$ (4). Measurement was made on an Enraf Nonius CAD4 diffractometer with graphite-monochromated Mo Kα radiation (λ = 0.710 69 Å) at 350 K. Accurate cell dimensions and crystal orientation matrices were determined by least-squares refinement of 25 reflections in the range 25.01 < 2θ < 29.79°. The intensities of 2549 (1231 unique) reflections were collected to a maximum 2θ value of 59.9° by the $\theta - 2\theta$ scan technique.

Structure Solution and Refinements. The structures were solved by direct methods (SIR97) and expanded using Fourier techniques.[21a] All refinements were made on F^2 by full-matrix least-squares method using program SHELXL97[21b] within Yadokari-XG 2009.[21c] For the RT phase of **3**, the S3···S4′ and S4···S3′ moieties coordinated to the Pt3−Pt3′ diplatinum unit are disordered over two positions and associated with the mirror plane, and the occupancy of each moiety was therefore fixed to 0.5. All non-hydrogen atoms in **3** were refined anisotropically except for the C3−C6, C9−C12 atoms of the n-pentyl groups, which were refined isotropically because of excessive thermal motions. For the HT phase of **3**, the S5, S6, S5′, and S6′ atoms coordinated to the Pt3−Pt3′ diplatinum unit were fixed at 0.5 occupancy similar to those for the RT phase of **3**. Besides, the S1···S2 and S3···S4 moieties coordinated to Pt1−Pt2 diplatinum unit also exhibit a positional disorder, which were refined with 0.5 occupancy. All non-hydrogen atoms in **3** were refined anisotropically except for the C3−C6, C9−C12 atoms of the n-pentyl groups that were refined isotropically because of high thermal motions, similarly to the RT phase. For the HT phase of **4**, the S1···S2′ and S2···S1′ moieties coordinated to the Pt1−Pt1′ diplatinum unit were disordered over two positions and associated with the mirror plane, and the occupancy of each moiety was therefore fixed at 0.5. All hydrogen atoms, except for those bonded to the carbon atoms placed on a mirror plane in the RT and HT phases of **3**, were placed in ideal positions and refined as riding atoms.

Electrical Transport Measurements. Direct current (DC) electrical conductivity measurements of **3** along the c axis (1-D chain direction) were made on several long prism-shaped single crystals in temperature range 80−400 K using a four-probe technique. Electrical contacts to the sample were made with gold paint to 25 mm ϕ gold wires. The sample was placed in a liquid nitrogen cryostat with helium as the exchange gas. The thermoelectric power of **3** was measured through a dynamical differential method using two sets of Au(Fe)−chromel

dx.doi.org/10.1021/ic102461z |Inorg. Chem. 2011, 50, 4368–4377

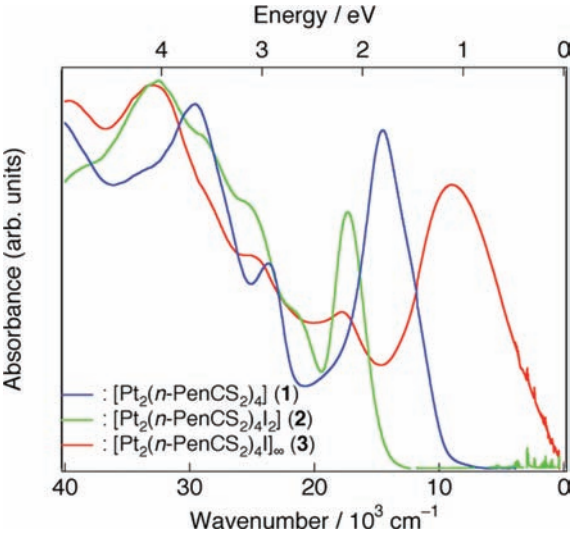

Figure 1. Electronic absorption spectra of $[Pt_2(n\text{-}PenCS_2)_4]$ (**1**), $[Pt_2(n\text{-}PenCS_2)_4I_2]$ (**2**), and $[Pt_2(n\text{-}PenCS_2)_4I]_\infty$ (**3**) in the solid-state (KBr disk for **1** and KI disks for **2** and **3**).

Table 3. Electronic Absorption Spectral Data of $[Pt_2(n\text{-}PenCS_2)_4]$ (1), $[Pt_2(n\text{-}PenCS_2)_4I_2]$ (2), and $[Pt_2(n\text{-}PenCS_2)_4I]_\infty$ (3) in the Solid-State[a]

compound	absorption band/10^3 cm^{-1}
1	14.5, 23.6, 29.6
2	17.3, 21.6 (sh), 25.3 (sh), 29.0(sh), 32.5
3	8.95, 17.8, 24.8 (sh), 32.9

[a] KBr disk for **1** and KI disks for **2** and **3**.

thermocouples (76 μm ϕ). The temperature gradient across the plate crystal along the *c* axis was increased using a heater up to ~0.5 K and simultaneously monitored by the thermocouples connected to separate nanovoltmeters. Absolute thermoelectric power was obtained after correction for the calibrated chromel.

3. RESULTS AND DISCUSSION

Saito et al. have previously reported detailed heat capacity data for **3**, obtained in an adiabatic calorimeter between 6−370 K.[18e] Their results revealed that **3** undergoes a first-order phase-transition at 207.4 K followed by a monotropic second-order phase-transition at 324 K on heating; thus defining three phases of low-temperature (LT), room-temperature (RT), and high-temperature (HT). Once **3** is transformed to the HT phase above 324 K it never returns to the initial phase even with cooling to liquid helium temperature. As already described in the introduction, analogous two-step phase transitions were observed in $[Pt_2(RCS_2)_4I]_\infty$ (R = *n*-Pr, *n*-Bu (**4**)) but all of these phase transitions are reversible.[18c,d] Below we present the results of a detail examination of the structural, electrical transport, and magnetic properties to elucidate the characteristics of the three ground states.

Electronic Absorption Spectra. The electronic absorption spectra of $[Pt_2(n\text{-}PenCS_2)_4]$ (**1**), $[Pt_2(n\text{-}PenCS_2)_4I_2]$ (**2**), and $[Pt_2(n\text{-}PenCS_2)_4I]_\infty$ (**3**) are shown in Figure 1, and the spectral data are summarized in Table 3.

The dominant feature of the absorption spectrum of **3** is an intense broad band centered at 8 950 cm^{-1} (1.11 eV) that is absent in the spectra of **1** and **2**. This lowest energy band can be attributed to the interdimer charge-transfer absorption, $d\sigma^{*0}d\sigma^{*2} \leftarrow d\sigma^{*1}d\sigma^{*1}$. This band is slightly shifted to higher energy relative to that of $[Pt_2(EtCS_2)_4I]_\infty$ (7 900 cm^{-1}, 0.98 eV).[11] This band extends to the mid-infrared region, thus relatively high electrical conductivity can be expected for **3**. The appearance of this band is consistent with **3** being in the mixed-valence state composed of Pt^{2+} and Pt^{3+}. The bands observed near 17 800 and 24 800 cm^{-1} for **3** are assigned to the $d\sigma^* \leftarrow \sigma(I)$ and $d\sigma^* \leftarrow d\pi^*$ transitions, respectively, similar to assignments made for $[Pt_2(EtCS_2)_4I]_\infty$.[11] The absorption bands at 17 300 and 21 600 cm^{-1} in **2** are also attributable to the $d\sigma^* \leftarrow \sigma(I)$ and $d\sigma^* \leftarrow d\pi^*$ transitions, respectively. The electronic absorption spectrum of **1** shows relatively intense bands at 14 500 and 23 600 cm^{-1}. The band at 14 500 cm^{-1}, however, disappears in solution. A similar electronic spectrum was observed for $[Pt_2(n\text{-}HexCS_2)_4]$[22] in the solid-state in which the lowest energy band was assigned to a transition arising from electronic interactions between dinuclear units stacked in a linear fashion within the crystal. Since similar stacking for **1** was revealed by X-ray analysis,[23] the band at 14 500 cm^{-1} should have the same origin. The band at 23 600 cm^{-1} could be assigned to the $p\sigma \leftarrow d\sigma^*$ transition by analogy with those of $[Pt_2(MeCS_2)_4]$[8a] and $[Pt_2(pop)_4]^{4-}$ (pop^{2-} = $P_2O_5H_2^{2-}$).[24]

Crystal Structure of $[Pt_2(n\text{-}PenCS_2)_4I]_\infty$ (3) in the RT Phase. The crystal structure of the RT phase of **3** at 250 K is shown in Figure 2.

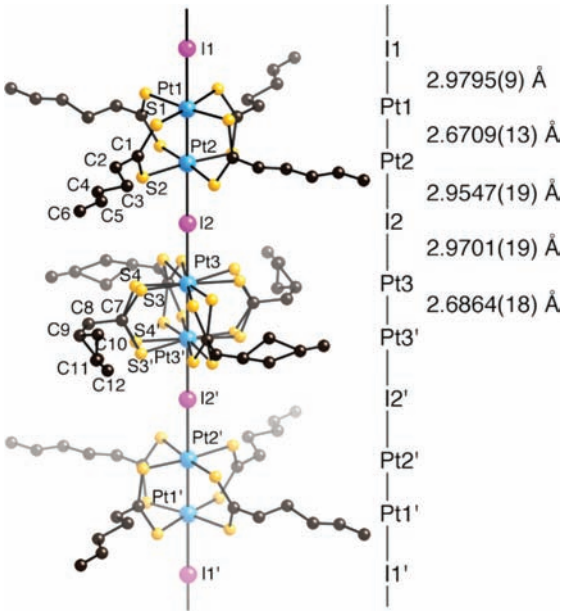

Figure 2. 1-D chain structure of $[Pt_2(n\text{-}PenCS_2)_4I]_\infty$ (**3**) in the RT phase at 250 K with an atomic numbering scheme and relevant interatomic distances.

X-ray diffraction measurements of **3** were performed using synchrotron radiation (22.011(5) keV, λ = 0.5633(1) Å) at the BL02B1 beamline of SPring-8, since the Bragg spots corresponding to the 3-fold periodic structure of a −Pt−Pt−I− period were extremely weak or undetectable because of the 3-fold periodic structure and excessive thermal motion in the *n*-pentyl groups of the ligands. In its RT phase **3** crystallizes in the tetragonal space group *I*4/*m*. The structure consists of neutral 1-D chains with a repeating −Pt−Pt−I− unit lying on the crystallographic 4-fold

dx.doi.org/10.1021/ic102461z |*Inorg. Chem.* 2011, 50, 4368–4377

axis parallel to the *c* axis. The unit cell dimension *c* along the 1-D chain direction consists of 3-fold of a −Pt−Pt−I− period. Crystallographic mirror planes perpendicular to the 1-D chain exist on the I1 atoms and the midpoint of Pt3 and Pt3′ atoms (i.e., z = 0, 0.5, 1). Consequently two PtS_4 planes in Pt3−Pt3′ diplatinum unit are disordered over two positions and the twisting directions of the two PtS_4 planes of adjacent Pt1−Pt2 diplatinum units in the 1-D chain are opposite to each other. Zamora et al. have reported the crystal structure of **3** in the RT phase in which the structure was solved in a lower symmetry space group *I*4 and therefore there is no disorder of the two PtS_4 planes of the central Pt−Pt unit.[25] On the other hand, similar 3-fold periodic structures with the same space group *I*4/*m* were observed in the RT phases of $[Pt_2(RCS_2)_4I]_\infty$ (R = *n*-Pr and *n*-Bu (**4**)) and our results for **3** are consistent with these observations.[13,12] Two platinum atoms are bridged by four dithiohexanato ligands in a paddle-wheel fashion with Pt−Pt distances of Pt1−Pt2 = 2.6709(13) and Pt3−Pt3′ = 2.6864(18) Å, which are about 0.21 Å shorter than the distances between the mean planes defined by the four sulfur atoms (2.876 and 2.907 Å), respectively. The twist angle between two PtS_4 planes are 21.9(2)° for a Pt1−Pt2 unit and ±21.6(4)° for a Pt3−Pt3′ unit, respectively. The three Pt−I distances are Pt1−I1 = 2.9795(9), Pt2−I2 = 2.9547(19), and Pt3−I2 = 2.9701(19) Å. Generally, a Pt^{2+}-I^- separation is greater than a Pt^{3+}−I^- separation since the d_{z^2} orbital of the Pt^{2+} site is occupied by a pair of electrons. Therefore, the difference between Pt−I bonds enables us to determine the valence state of Pt atoms. Taking into account the small but significant differences in the Pt−I and Pt−Pt distances, the valence-ordered state of the platinum atoms in the 3-fold periodic structure may be regarded as an extreme model of $—I^-—Pt^{2+}—Pt^{3+}—I^-—Pt^{2.5+}—Pt^{2.5+}—I^-$-$Pt^{3+}—Pt^{2+}—I^-—$. In such a valence state, the unpaired electrons on the adjacent Pt^{3+} sites are expected to take a singlet state because of the strong antiferromagnetic coupling through the bridging iodine atom. However **3** is a paramagnet in the RT and HT phases. Furthermore, as will be described in next section, diffuse scattering with the 2-fold periodicity of a −Pt−Pt−I− period was observed in the RT and HT phases, indicating the presence of the valence fluctuation having the 2-fold periodicity of a −Pt−Pt−I− period. In its RT phase **3** should consequently be assigned to the valence-ordered state close to the AV state. Adjacent $Pt_2(CS_2)_4$ units of Pt1−Pt2 and Pt3−Pt3′ are twisted by about 26° from the eclipsed arrangement. The *n*-pentyl groups of the dithiohexanato ligands in the Pt1−Pt2 unit have the *anti*-like form, whereas those of the Pt3−Pt3′ unit take the *gauche*-like form. Therefore, the origin of 3-fold periodic structure cannot be attributed to the valence ordering of the platinum atoms, but to both the twist of the adjacent diplatinum units and the difference in the conformation of the dithiohexanato ligands.

X-ray Diffraction Photographs. In our previous studies, it has been demonstrated that the lattice periodicity along the 1-D chain direction of $[Pt_2(RCS_2)_4I]_\infty$ (R = *n*-Pr, *n*-Bu(**4**)) changes with the two-step first- or higher-order phase-transitions.[13,12] Furthermore, the MMX chain compounds are expected to exhibit diffuse scattering arising from the valence ordering, since these compounds can potentially take a variety of valence-ordered states as described in the introduction. To examine the lattice periodicity of the 1-D chain in each phase, X-ray diffraction photographs of **3** in the HT, RT, and LT phases were measured using synchrotron radiation at the BL02B1 beamline of SPring-8,

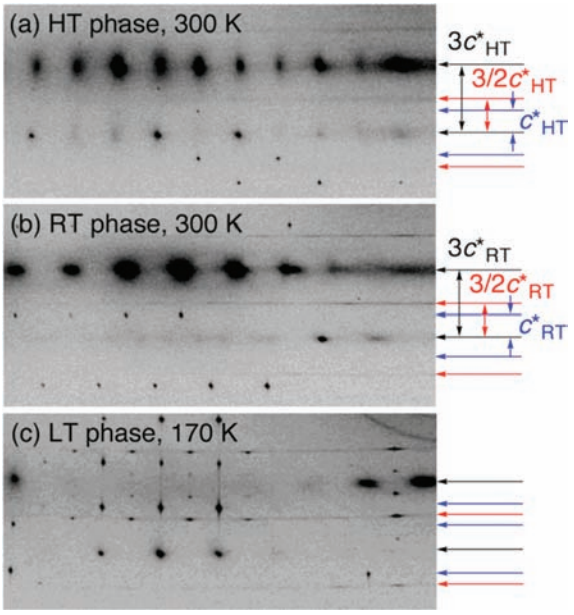

Figure 3. Portions of X-ray oscillation photographs of $[Pt_2(n\text{-}PenCS_2)_4I]_\infty$ (**3**) in each phase taken with an oscillation angle of 3° around *c* axis. Axis *c** (1-D chain direction) is vertical. The X-ray diffraction experiment of the supercooled HT phase was carried out at 300 K using a crystal once heated to 350 K.

and the results are shown in Figure 3 and Supporting Information, Figures S1−S3. The X-ray diffraction experiment of the supercooled HT phase was carried out at 300 K using a crystal once heated to 350 K.

In Figure 3 (b) taken in the RT phase, the strong Bragg spots are observed at the position of $3c^*_{RT}$, where the c^*_{RT} is the reciprocal lattice parameter along the 1-D chain in the RT phase, corresponding to the basic periodicity of a −Pt−Pt−I− period, whereas the weak Bragg spots have appeared at the position of c^*_{RT}, which is consistent with the periodicity of 1-D chain being 3-fold of a −Pt−Pt−I− period. The weak Bragg spots corresponding to c^*_{RT} are also observed in the HT and LT phases, and it is found that the 3-fold periodic structure observed in the RT phase remains in the HT and LT phases. In Figure 3 (a) and (b), in addition to the Bragg spots corresponding to the 3-fold periodic structure, diffuse streaks are observed at the reciprocal positions of 3/2 c^*_{RT} corresponding to 2-fold of a −Pt−Pt−I− period. The observed diffuse scattering is believed to originate from 1-D periodic arrangement, since the intensity of diffuse scattering does not depend on the orientation of the crystal. Similar diffuse scattering with the 2-fold repetition length was observed for $[Pt_2(RCS_2)_4I]_\infty$ (R = Et, *n*-Pr, and *n*-Bu(**4**)), which is attributed to the dynamical valence-ordering with the 2-fold periodicity corresponding to ACP or CDW existing in an extremely short time scale.[26,13,12] Similarly, the diffuse scattering observed in **3** can therefore be attributed to the 2-fold periodicity corresponding to dynamic ACP or CDW state. In Figure 3 (c), the diffuse scattering observed in the RT and HT phases changes to the distinct Bragg spots in the LT phase, which indicates that the valence fluctuation having the 2-fold periodicity of a −Pt−Pt−I− period has frozen and then the 3-D static valence ordering develops in the LT phase. From these facts, it is found that the LT phase takes 6-fold periodic structure including the 2-fold periodic valence ordering, in addition to the 3-fold

dx.doi.org/10.1021/ic102461z |*Inorg. Chem.* 2011, 50, 4368–4377

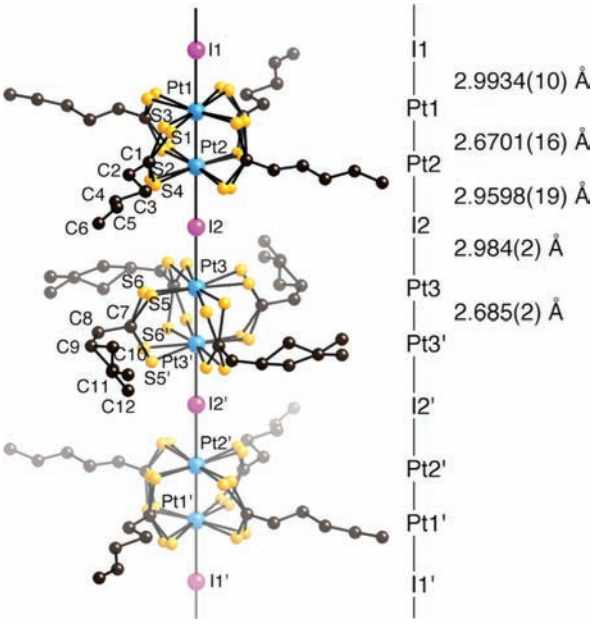

Figure 4. 1-D chain structure of $[Pt_2(n\text{-}PenCS_2)_4I]_\infty$ (**3**) in the HT phase at 270 K with an atomic numbering scheme and relevant interatomic distances.

periodic structure arising from the structural difference between the diplatinum units. A similar 6-fold periodic structure has been observed in the semiconducting region of $[Pt_2(n\text{-}PrCS_2)_4I]_\infty$.[13] However, the crystal structure determination of the superstructure corresponding to 6-fold of a −Pt−Pt−I− period was unsuccessful.

Crystal Structure of $[Pt_2(n\text{-}PenCS_2)_4I]_\infty$ (3) in the Supercooled HT Phase. As already described, **3** undergoes a monotropic phase transition at 324 K on heating.[18e] To reveal the origin of the monotropic nature of the RT−HT phase transition, the crystal structure analysis of the supercooled HT phase was carried out at 270 K using a crystal once heated to 350 K.

The crystal structure of **3** in the HT phase is shown in Figure 4. In contrast to the HT phase of $[Pt_2(RCS_2)_4I]_\infty$ (R = *n*-Pr and *n*-Bu (**4**) (see next section)) having the 1-fold periodicity of a −Pt−Pt−I− period,[13] the structure of **3** in the HT phase takes the same space group *I*4/*m* and a similar 3-fold periodic structure as its RT phase.

The two Pt−Pt distances are Pt1−Pt2 = 2.6701 (16) and Pt3−Pt3′ = 2.685 (2) Å, while the three Pt−I distances are Pt1−I1 = 2.9934 (10), Pt2−I2 = 2.9598 (19), and Pt3−I2 = 2.984 (2) Å, respectively. These distances are close to those of the RT phase at 250 K. Similar to the RT phase of **3**, the ligand moieties including sulfur atoms of Pt3−Pt3′ units are disordered on two positions with the twist angle of ±21.5 (4)° because of the crystallographic mirror planes perpendicular to the 1-D chain existing on the midpoint of Pt3 and Pt3′ atoms. Furthermore, there is a distinct structural difference between the RT and HT phases. It is found that two PtS_4 planes of the Pt1−Pt2 diplatinum unit are disordered over two positions with 0.5 occupancy. These twist angles between two PtS_4 planes are 31.7 (4)° and 11.6 (5)°, respectively. The crystal structure of **3** in the HT phase has also been reported but the structure was solved in the lower symmetry space group *C*2/*m* with the 3-fold periodicity of a −Pt−Pt−I−.[25] The reported twist angles between two PtS_4 planes in the diplatinum units with and

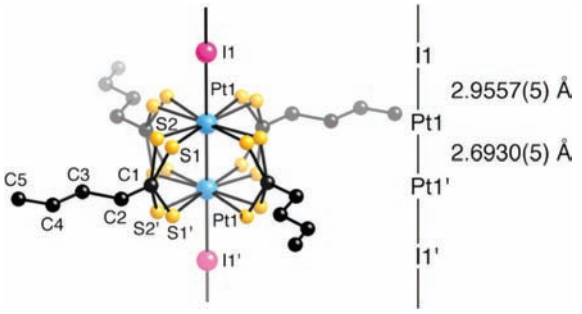

Figure 5. 1-D chain structure of $[Pt_2(n\text{-}BuCS_2)_4I]_\infty$ (**4**) in the HT phase at 350 K with an atomic numbering scheme and relevant interatomic distances.

without a mirror plane are 0° and 15.6°, respectively, and the disorder of the two PtS_4 planes has not been observed. On the other hand, in the case of $[Pt_2(RCS_2)_4I]_\infty$ (R = *n*-Pr and *n*-Bu (**4**)), the unit cell dimension *c* along the 1-D chain direction changes from 3-fold of a −Pt−Pt−I− period in the RT phase to 1-fold in the HT one, and the two PtS_4 planes of all the diplatinum units are disordered in two positions.[13] These facts are consistent with our result observed for the HT phase in **3**, and therefore the RT−HT phase transition found in **3** is believed to originate from the fact that the two PtS_4 planes in all the diplatinum units are disordered in two positions in the HT phase. The valence-ordered state of the platinum atoms in the HT phase may be regarded not as $—I^-—Pt^{2+}—Pt^{3+}\text{-}I^-—Pt^{2.5+}—Pt^{2.5+}—I^-\text{-}Pt^{3+}—Pt^{2+}—I^-—$ but as the valence-ordered state close to the AV state similarly to the RT phase. Adjacent $Pt_2(CS_2)_4$ units of Pt1−Pt2 and Pt3−Pt3′ are twisted by about 28° from the eclipsed arrangement.

Crystal Structure of $[Pt_2(n\text{-}BuCS_2)_4I]_\infty$ (4) in HT Phase. $[Pt_2(n\text{-}BuCS_2)_4I]_\infty$ (**4**) is revealed from the heat capacity measurement to undergo two-step first-order phase transitions at 213.5 and 323.5 K on heating, respectively, and three phases of the low-temperature (LT), room-temperature (RT), and high-temperature (HT) phases exist.[18d] The crystal structures of **4** in the RT and LT phases have been reported previously.[12] To compare with the structure of **3** in the HT phase, the crystal structure analysis of **4** in the HT phase has been carried out at 350 K. The crystal structure of **4** in the HT phase is shown in Figure 5.

4 crystallizes in the tetragonal space group *I*4/*m*. The RT phase of **4** has the same 3-fold periodic structure with the space group *I*4/*m* as the RT phases of the compound **3** and $[Pt_2(n\text{-}PrCS_2)_4I]_\infty$; however, the periodicity of the crystal lattice in the 1-D chain direction in the HT phase of **4** is found to change to 1-fold while keeping the same space group. The structural differences of the dithiopentanato ligands of **4** between the adjacent diplatinum units observed in the RT phase are removed in the HT phase. This structural change to the HT phase is analogous to that observed for $[Pt_2(n\text{-}PrCS_2)_4I]_\infty$.[13] The Pt1−Pt1′ distance is 2.6930 (5) Å, which is 0.22 Å shorter than the distance between the mean planes defined by the four sulfur atoms (2.916 (3) Å). Crystallographic mirror planes perpendicular to the 1-D chain exist on the I1 atoms and the midpoint of Pt1 and Pt1′ atoms (i.e., z = 0, 0.5, 1). Therefore, the bridging iodine atom exists at the midpoint of the diplatinum units (Pt1−I1 = 2.9557 (5) Å), and two PtS_4 planes are disordered on two positions with the twist angle of ±18.41 (9)°.

dx.doi.org/10.1021/ic102461z |*Inorg. Chem.* 2011, 50, 4368–4377

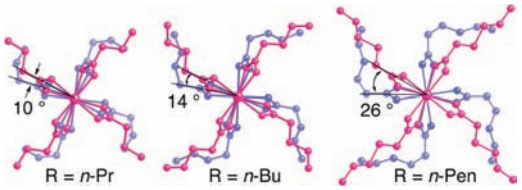

Figure 6. Comparison of crystal structures of $[Pt_2(RCS_2)_4I]_\infty$ (R = *n*-Pr, *n*-Bu (**4**), *n*-Pen (**3**)) viewed along the *c* axis (1-D chain direction).

Comparison of Crystal Structures of $[Pt_2(RCS_2)_4I]_\infty$ (R = *n*-Pr, *n*-Bu (4), and *n*-Pen (3)). Since the solid-state properties of **3** differ from those of other MMX compounds, we discuss the origin of these differences based on the comparison of the crystal structures. $[Pt_2(RCS_2)_4I]_\infty$ (R = *n*-Pr, *n*-Bu (**4**), and *n*-Pen (**3**)) having a similar 3-fold periodic structure with the same space group of *I*4/*m* in the RT phase undergo the RT−HT phase transition at temperature above 300 K.[18c−e] The periodicity for the former two compounds changes to 1-fold with a −Pt−Pt−I− period in the HT phase through a first-order phase transition, whereas the compound **3** which undergoes the monotropic phase transition retains the 3-fold periodic structure even at the HT phase. The RT−HT phase transition temperature of $[Pt_2(RCS_2)_4I]_\infty$ decreases in order of R = Me (372 K),[18a] R = *n*-Pr (358.8 K),[18c] and R = *n*-Bu (**4**) (323.5 K),[18d] but that of R = *n*-Pen (**3**) is 324 K which is almost the same value as for **4**.[18e] To clarify the origin of the difference of these properties, we discuss it based on the comparison of the crystal structures. The *c* axis projection of **3** in the RT phase is shown in Figure 6, together with those of $[Pt_2(RCS_2)_4I]_\infty$ (R = *n*-Pr, *n*-Bu (**4**)).[13,12]

In all of these compounds, the unit cell dimension *c* along the 1-D chain direction in the RT phases consists of three −Pt−Pt−I− units, and two kinds of diplatinum units exist in the crystal. The differences between the two kinds of the diplatinum units comprise both the twist of the adjacent diplatinum units and the difference in the conformation of the alkyl group of the dithiocarboxylato ligands. The molecule colored in blue is disordered in two PtS_4 planes, whereas the two PtS_4 planes colored in red are ordered. Twist angle between two kinds of adjacent $Pt_2(CS_2)_4$ units in $[Pt_2(RCS_2)_4I]_\infty$ increases in order of R = *n*-Pr (10°),[13] R = *n*-Bu (**4**) (14°),[12] and R = *n*-Pen (**3**) (26°), and the differences in the ligand conformation between two kinds of the diplatinum units increase in the same order. Therefore, it is considered that **3** retains a 3-fold periodic structure in the HT phase, since the twisting angle and difference in the ligand conformation between two kinds of the diplatinum units are too large to take the 1-fold periodicity of a −Pt−Pt−I− period. Taking into consideration the disorder of two PtS_4 planes in the diplatinum unit observed in the HT phase of $[Pt_2(RCS_2)_4I]_\infty$ (R = Me, *n*-Pr and *n*-Bu (**4**)),[9c,13] it is assumed that the disorder of two PtS_4 planes in **3** occurs in all of the diplatinum units with the RT−HT phase transition. Actually, as already described, the validity of this hypothesis is confirmed by the crystal structure analysis of the HT phase. Saito et al. have reported on the origin of these phase transitions from a detailed specific heat measurement of a series of the MMX compounds as follows.[18c,d] In the case of $[Pt_2(RCS_2)_4I]_\infty$ (R = *n*-Pr, *n*-Bu (**4**)), the entropy reserved as the disorder in alkyl chains of RCS_2 ligands in the RT phase is transferred to the $Pt_2(CS_2)_4$ units with the RT−HT phase transition, and the 3-fold periodic structure in the RT phase changes to the 1-fold periodicity in the HT phase with the disorder of all of two PtS_4 planes. In contrast to these results, the entropy change of the RT−HT transition of **3** is effectively zero

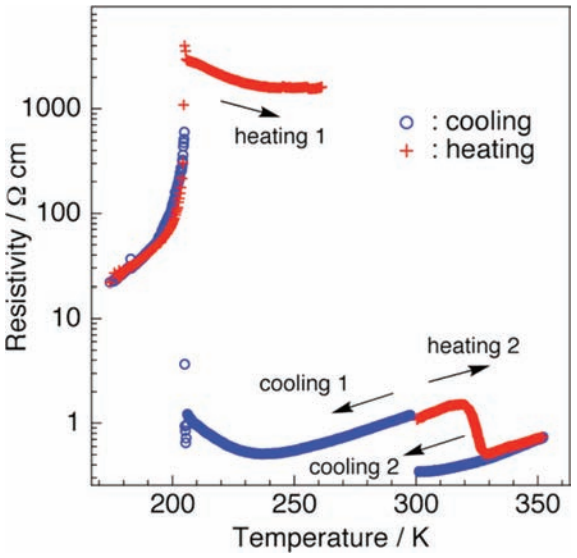

Figure 7. Temperature dependence of the electrical resistivity of $[Pt_2(n\text{-}PenCS_2)_4I]_\infty$ (**3**) measured along the chain axis *c* under different procedures.

since a phase transition without entropy change is possible because of the reserved entropy in the alkyl chain being much larger than that required for the disordering of all the $Pt_2(CS_2)_4$ units.[18e] The $\Delta G = G_{RT} - G_{HT}$ obtained for **3** is positive, indicating that the RT phase is not stable but metastable even below 324 K, which is consistent with the monotropic nature of the RT−HT phase transition.[18e] The phase transition observed here is therefore that from a metastable RT phase to a stable HT phase.

Transport Properties. Temperature dependence of the electrical resistivity of **3** along the 1-D chain is represented in Figure 7.

The electrical conductivity of **3** at room temperature is a relatively high value of 0.84 S cm^{-1}, similar to that previously reported for the same compound (0.3−1.4 S cm^{-1})[25] but is lower than those of $[Pt_2(RCS_2)_4I]_\infty$ (R = Me (∼13 S cm^{-1}),[10] Et (5−30 S cm^{-1}),[11] and *n*-Bu (**4**) (17−43 S cm^{-1})).[12] The electrical resistivity in the cooling 1 process decreases with lowering temperature from RT and reaches a minimum around 235 K. The observed minimum in ρ indicates that **3** undergoes a metal−semiconductor transition at T_{M-S} = 235 K, which is lower than the minimum observed for the same compound (255−270 K).[25] The compound **3** is the most stable metallic state second to $[Pt_2(EtCS_2)_4I]_\infty$ (T_{M-S} = 205 K).[11] The diffuse scattering observed in the metallic state in **3** indicates that the valence fluctuation plays an essential role in the appearance of the metallic state, similarly to that observed in $[Pt_2(EtCS_2)_4I]_\infty$.[26] The electrical resistivity exhibits a resistivity jump with the first-order RT−LT phase transition near 205 K and then decreases with lowering temperature. With increasing temperature from 170 K, the electrical resistivity increases and shows a resistivity jump at about 205 K, and the electrical resistivity in the heating 1 process in the RT phase is 3 orders of magnitude larger than that of the cooling 1 process in the RT phase, which could be due to the microcracks formed in the crystal during the transformation. The resistivity in the heating 2 process measured using another as-grown crystals exhibits rapid decrease with the phase transition in the temperature range of 320−328 K, but the resistivity in the cooling 2 process from 350 K does not show the HT−RT phase transition. This behavior is consistent with the tendency

dx.doi.org/10.1021/ic102461z |*Inorg. Chem.* 2011, 50, 4368–4377

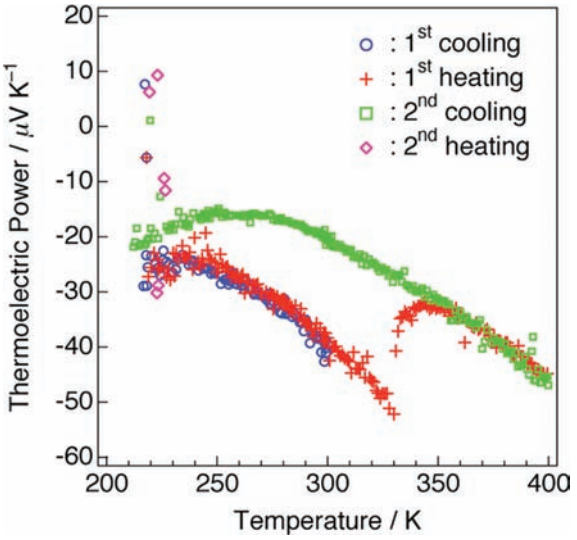

Figure 8. Temperature dependence of absolute thermoelectric power of $[Pt_2(n\text{-}PenCS_2)_4I]_\infty$ (**3**) measured along the chain axis *c*.

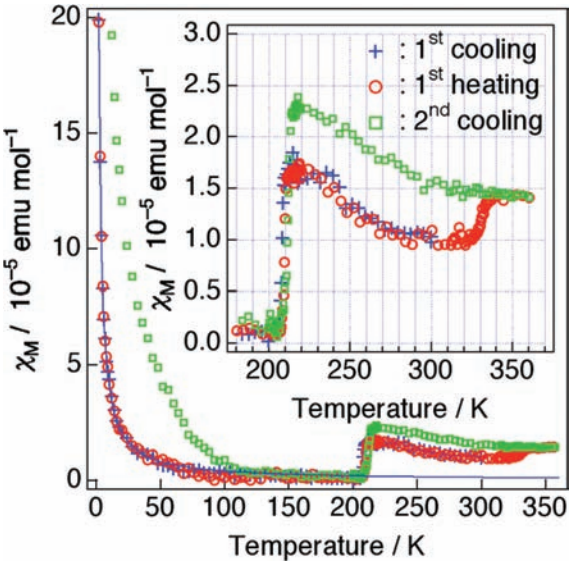

Figure 9. Temperature dependence of the magnetic susceptibility χ_M of $[Pt_2(n\text{-}PenCS_2)_4I]_\infty$ (**3**). The solid line represents the fitting to estimate the impurity spin concentration.

observed in the heat capacity measurement[18e] and indicates that the phase transition is monotropic. Unlike the previously reported electrical resistivity for the same compound,[25] the resistivities in the heating 2 and cooling 2 processes in the HT phase coincide with each other.

As shown in Figure 8, the thermoelectric power *S* in the first cooling process increases with lowering the temperature and exhibits a maximum at 235 K before rapidly increasing with the first-order RT−LT phase transition near 205 K. On first heating, *S* increases through the same pathway as the first cooling process, and then exhibits an increase at the RT−HT phase transition in the temperature range of 330−344 K. Upon second cooling from 400 K, *S* does not show the rapid decrease associated with the RT−HT phase transition and exhibits a round maximum near 260 K. The observed irreversibility is consistent with the tendency observed in the heat capacity and resistivity measurements. Thermoelectric power measurement is less sensitive to microcracks within a crystal compared to the resistivity measurements. Therefore, it is considered that the rapid increase in *S* observed at the RT−LT phase transition would not only be the influence of microcracks produced in the crystal but also the opening of the band gap. This behavior is consistent with the freezing of the valence fluctuation with the RT−LT phase transition observed in the diffuse scattering experiments. The carrier in the RT and HT phases is an electron since *S* shows negative values. In a 1-D tight-binding picture, the temperature dependence of *S* is given by

$$S = -\frac{\pi^2 k_B^2 T}{6|e||t|}\frac{\cos\frac{1}{2}\pi\rho}{1-\cos^2\frac{1}{2}\pi\rho} \quad (1)$$

where *e* is the electron charge, ρ is the electron density in the band ($\rho = 1$ for one electron per site), and *t* is the transfer integral ($4t$ being the bandwidth *W*).[27] If MMX units form a metallic band, it will be an effective half-filled band mainly composed of the Pt−Pt $d\sigma^*$−I pz combination as the present compound has formally one unpaired electron per MMX unit. Within the tight-binding approximation, the thermoelectric power of the half-filled band ($\rho = 1$) would give a temperature-independent value of zero. *S* in the temperature range of 210−400 K varies from −15 to −50 μV K^{-1}, and exhibits temperature dependence. This behavior is not consistent with the metallic behavior above 235 K observed in the resistivity measurement. The origin of the temperature dependence may be attributed to the scattering of electrons by phonons and/or impurity, but it is unclear. The observed temperature of the maximum in *S* coincides with metal−semiconductor transition temperature T_{M-S} = 235 K determined from the resistivity measurement.

Magnetic Property. The temperature dependence of the magnetic susceptibility χ_M of **3** is shown in Figure 9.

The magnetic susceptibility in the RT and HT phases is of the order of 1−2.5 × 10^{-5} emu mol^{-1}. The low susceptibility is consistent with Pauli paramagnetism as one may expect for a conductor. The enhanced value may be due to considerable electron−electron correlation. The tail, observed in the χ_M versus *T* plot below 30 K, can account for paramagnetic impurities and/or lattice and end-of-chains defects. The impurity spin concentration is estimated to be 0.11% as the $S = 1/2$ Curie spin. The most striking feature is an abrupt decrease in the χ_M to the spin-singlet state with the first-order RT−LT phase transition. A similar temperature dependence of χ_M has been observed in $[Pt_2(n\text{-}BuCS_2)_4I]_\infty$ (**4**), in which the spin singlet state appears with the first-order RT−LT phase transition from the AV state to the ACP state around 205 K.[12] As described in the X-ray diffraction, the compound **3** in the RT phase exhibits the diffuse scattering corresponding to a 2-fold repetition length of a −Pt−Pt−I− period, in addition to the main Bragg spots, which changes to the Bragg spots in the LT phase. Therefore, the compound **3** is considered to take the spin singlet state with the first-order phase transition from the valence ordered state close to AV state in the RT phase to the ACP or CDW state in the LT phase. Taking into account the valence-ordered state of $[Pt_2(RCS_2)_4I]_\infty$ (R = Et, *n*-Bu(**4**)) in the LT phase,[12] the most probable ground state of **3** would be the ACP state of —Pt^{2+}−Pt^{3+}-I^--Pt^{3+}−Pt^{2+}—I^-—.

dx.doi.org/10.1021/ic102461z |*Inorg. Chem.* 2011, 50, 4368–4377

The temperature dependence of χ_M in the first heating process below RT coincides with that in the first cooling process, but exhibits a slight increase at the monotropic phase transition to the HT phase in the temperature range of 324−335 K. It is confirmed from the result of the second cooling process that the HT phase does not return to the RT phase in agreement with the results with the heat capacity measurement and transport properties.[18e] The magnetic behavior observed in **3** is consistent with the previously reported spin susceptibility of the same compound obtained by electron paramagnetic resonance (EPR) measurement.[28] Saito et al. have also reported that the HT phase of **3** undergoes the successive phase transition of HT phase−MT′ phase−LT′ phase (MT, middle temperature) on cooling separated by a first-order phase transition at 220.5 K and a higher-order phase transition at 173 K which has a large tail down to about 120 K, respectively.[18e] Consistent with these results, χ_M exhibits an abrupt decrease to the spin-singlet state with the HT−MT′ phase transition and then shows a rapid increase with the MT′−LT′ phase transition below about 120 K. Therefore, it is reasonable to assume that the structural modulation occurs with the higher-order MT′−LT′ phase transition, and the magnetic defects that give free spins would be formed in the 1-D chain.

4. CONCLUSION

To examine the effects of the elongation of the alkyl chain in the dithiocarboxylate ligands on the crystal structure and 1-D electronic system, we studied the synthesis, crystal structures, and solid-state properties of $[Pt_2(n\text{-}PenCS_2)_4I]_\infty$ (**3**). As the results, we have demonstrated that the interplay between electronic degrees of freedom and molecular dynamics causes the structural phase-transition accompanying electronic and magnetic transitions. **3** undergoes two phase transitions at 207 and 324 K on heating similarly to $[Pt_2(RCS_2)_4I]_\infty$ (R = *n*-Pr[13] and *n*-Bu (**4**)[12]), where that at 207 K is first order and reversible but that at 324 K is monotropic, that is, irreversible. Single-crystal X-ray structure determinations in conjunction with diffuse scattering experiments in the three states clearly demonstrate the changes in the periodicities and the localization of charges which explain the respective metal−insulator paramagnetic-diamagnetic and metal−metal paramagnetic-paramagnetic transitions observed. These transitions appear to be governed by the degree of the relative movement of the PtS_4 moieties of the paddle wheel building blocks and by the degree of the motion of the platinum and iodine atoms in the chains. The presence of disorder of the long alkyl groups, which is quite likely to be the source of the remaining entropy even at very low temperatures, is reminiscent of those observed in discotic liquid crystals formed on similar structural building blocks.

■ ASSOCIATED CONTENT

Ⓢ Supporting Information. X-ray crystallographic information file in CIF format for compounds **3** and **4**. X-ray diffraction pattern for **3** in the HT, RT, and LT phases. This material is available free of charge via the Internet at http://pubs.acs.org.

■ AUTHOR INFORMATION

Corresponding Author

*Phone: (+81)791-58-0153 (M.M.). Fax: (+81)791-58-0154 (M.M.). E-mail: mitsumi@sci.u-hyogo.ac.jp (M.M.).

Present Addresses

‖Division of Chemistry, Graduate School of Science, Kyoto University, Kitashirakawa-Oiwakecho, Sakyo-ku, Kyoto, 606-8502, Japan.

Notes

⊥Present position: Professor Emeritus.

■ ACKNOWLEDGMENT

This work was supported by a Grants-in-Aids for Scientific Research (10740307 and 20550130) and Priority Areas "Metal-Assembled Complexes" (11136244) from the Ministry of Education, Culture, Sports, Science and Technology, Japan, the Mitsubishi Chemical Corporation Fund, Grant for Basic Science Research Projects of the Sumitomo Foundation and the CNRS-France. This study was supported by the SPring-8 (2010B1503). We also thank the Instrument Center, the Institute for Molecular Science, for the use of X-ray diffractometer (Rigaku AFC7 Mercury CCD diffractometer).

■ REFERENCES

(1) (a) Yamada, S.; Tsuchida, R. *Bull. Chem. Soc. Jpn.* **1956**, *29*, 894–898. (b) Clark, R. J. H.; Franks, M. L.; Trumble, W. R. *Chem. Phys. Lett.* **1976**, *41*, 287–292.

(2) Krogmann, K. *Angew. Chem., Int. Ed. Engl.* **1969**, *8*, 35–42.

(3) (a) Comès, R.; Lambert, M.; Zeller, H. R. *Phys. Status Solidi B* **1973**, *58*, 587–592. (b) Comès, R.; Lambert, M.; Launois, H.; Zeller, H. R. *Phys. Rev. B* **1973**, *8*, 571–575.

(4) For direct M−M chain systems, see: (a) Zeller, H. R.; Beck, A. *J. Phys. Chem. Solids* **1974**, *35*, 77–80. (b) Kobayashi, A.; Sasaki, Y.; Shirotani, I.; Kobayashi, H. *Solid State Commun.* **1978**, *26*, 653–656. (c) Bera, J. K.; Dunbar, K. R. *Angew. Chem., Int. Ed.* **2002**, *41*, 4453–4457. (d) Prater, M. E.; Pence, L. E.; Clérac, R.; Finniss, G. M.; Campana, C.; Auban-Senzier, P.; Jérome, D.; Canadell, E.; Dunbar, K. R. *J. Am. Chem. Soc.* **1999**, *121*, 8005–8016. (e) Sakai, K.; Ishigami, E.; Konno, Y.; Kajiwara, T.; Ito, T. *J. Am. Chem. Soc.* **2002**, *124*, 12088–12089. (f) Mitsumi, M.; Goto, H.; Umebayashi, S.; Ozawa, Y.; Kobayashi, M.; Yokoyama, T.; Tanaka, H.; Kuroda, S.; Toriumi, K. *Angew. Chem., Int. Ed.* **2005**, *44*, 4164–4168. (g) Uemura, K.; Fukui, K.; Nishikawa, H.; Arai, S.; Matsumoto, K.; Oshio, H. *Angew. Chem., Int. Ed.* **2005**, *44*, 5459–5464. (h) Mitsumi, M.; Ueda, H.; Furukawa, K.; Ozawa, Y.; Toriumi, K.; Kurmoo, M. *J. Am. Chem. Soc.* **2008**, *130*, 14102–14104.

(5) Wolffram, H. Dissertation, University of Königsberg, Germany, 1900.

(6) (a) Takaishi, S.; Yamashita, M. *Chem. Lett.* **2008**, *37*, 382–387. (b) Yamashita, M.; Takaishi, S. *Chem. Commun.* **2010**, *46*, 4438–4448.

(7) (a) Che, C.-M.; Herbstein, F. H.; Schaefer, W. P.; Marsh, R. E.; Gray, H. B. *J. Am. Chem. Soc.* **1983**, *105*, 4604–4607. (b) Kurmoo, M.; Clark, R. J. H. *Inorg. Chem.* **1985**, *24*, 4420–4425. (c) Clark, R. J. H.; Kurmoo, M.; Dawes, H. M.; Hursthouse, M. B. *Inorg. Chem.* **1986**, *25*, 409–412. (d) Butler, L. G.; Zietlow, M. H.; Che, C.-M.; Schaefer, W. P.; Sridhar, S.; Grunthaner, P. J.; Swanson, B. I.; Clark, R. J. H.; Gray, H. B. *J. Am. Chem. Soc.* **1988**, *110*, 1155–1162. (e) Stroud, M. A.; Drickamer, H. G.; Zietlow, M. H.; Gray, H. B.; Swanson, B. I. *J. Am. Chem. Soc.* **1989**, *111*, 66–72. (f) Mitani, T.; Wada, Y.; Yamashita, M.; Toriumi, K.; Kobayashi, A.; Kobayashi, H. *Synth. Met.* **1994**, *64*, 291–294. (g) Yamashita, M.; Miya, S.; Kawashima, T.; Manabe, T.; Sonoyama, T.; Kitagawa, H.; Mitani, T.; Okamoto, H.; Ikeda, R. *J. Am. Chem. Soc.* **1999**, *121*, 2321–2322.(h) Matsuzaki, H.; Matsuoka, T.; Kishida, H.; Takizawa, K.; Miyasaka, H.; Sugiura, K.; Yamashita, M.; Okamoto, H. *Phys. Rev. Lett.* **2003**, *90*, 046401 (4 pages). (i) Mastuzaki, H.; Kishida, H.; Okamoto, H.; Takizawa, K.; Matsunaga, S.; Takaishi, S.; Miyasaka, H.; Sugiura, K.; Yamashita, M. *Angew. Chem., Int. Ed.* **2005**, *44*, 3240–3243. (j) Yamashita, M.; Takaishi, S.; Kobayashi, A.; Kitagawa, H.; Matsuzaki, H.; Okamoto, H. *Coord. Chem. Rev.* **2006**,

250, 2335–2346. (k) Iguchi, H.; Takaishi, S.; Kajiwara, T.; Miyasaka, H.; Yamashita, M.; Matsuzaki, H.; Okamoto, H. *J. Am. Chem. Soc.* **2008**, *130*, 17668–17669.

(8) (a) Bellitto, C.; Flamini, A.; Gastaldi, L.; Scaramuzza, L. *Inorg. Chem.* **1983**, *22*, 444–449. (b) Bellitto, C.; Dessy, G.; Fares, V. *Inorg. Chem.* **1985**, *24*, 2815–2820. (c) Clark, R. J. H.; Walton, J. R. *Inorg. Chim. Acta* **1987**, *129*, 163–171.

(9) (a) Yamashita, M.; Wada, Y.; Toriumi, K.; Mitani, T. *Mol. Cryst. Liq. Cryst.* **1992**, *216*, 207–212. (b) Shirotani, I.; Kawamura, A.; Yamashita, M.; Toriumi, K.; Kawamura, H.; Yagi, T. *Synth. Met.* **1994**, *64*, 265–270.(c) Ozawa, Y.; Kim, M.; Takata, K.; Toriumi, K. unpublished results.

(10) Kitagawa, H.; Onodera, N.; Sonoyama, T.; Yamamoto, M.; Fukawa, T.; Mitani, T.; Seto, M.; Maeda, Y. *J. Am. Chem. Soc.* **1999**, *121*, 10068–10080.

(11) Mitsumi, M.; Murase, T.; Kishida, H.; Yoshinari, T.; Ozawa, Y.; Toriumi, K.; Sonoyama, T.; Kitagawa, H.; Mitani, T. *J. Am. Chem. Soc.* **2001**, *123*, 11179–11192.

(12) Mitsumi, M.; Kitamura, K.; Morinaga, A.; Ozawa, Y.; Kobayashi, M.; Toriumi, K.; Iso, Y.; Kitagawa, H.; Mitani, T. *Angew. Chem., Int. Ed.* **2002**, *41*, 2767–2771.

(13) Mitsumi, M.; Umebayashi, S.; Ozawa, Y.; Toriumi, K.; Kitagawa, H.; Mitani, T. *Chem. Lett.* **2002**, *31*, 258–259.

(14) Mitsumi, M.; Yoshida, Y.; Kohyama, A.; Kitagawa, Y.; Ozawa, Y.; Kobayashi, M.; Toriumi, K.; Tadokoro, M.; Ikeda, N.; Okumura, M.; Kurmoo, M. *Inorg. Chem.* **2009**, *48*, 6680–6691.

(15) (a) Wakabayashi, Y.; Kobayashi, A.; Sawa, H.; Ohsumi, H.; Ikeda, N.; Kitagawa, H. *J. Am. Chem. Soc.* **2006**, *128*, 6676–6682. (b) Otsubo, K.; Kobayashi, A.; Kitagawa, H.; Hedo, M.; Uwatoko, Y.; Sagayama, H.; Wakabayashi, Y.; Sawa, H. *J. Am. Chem. Soc.* **2006**, *128*, 8140–8141.

(16) (a) Borshch, S. A.; Prassides, K.; Robert, V.; Solonenko, A. O. *J. Chem. Phys.* **1998**, *109*, 4562–4568. (b) Robert, V.; Petit, S.; Borshch, S. A. *Inorg. Chem.* **1999**, *38*, 1573–1578. (c) Calzolari, A.; Alexandre, S. S.; Zamora, F.; Felice, R. D. *J. Am. Chem. Soc.* **2008**, *130*, 5552–5562.

(17) (a) Nakano, S.; Kitagawa, Y.; Kawakami, T.; Yamaguchi, K. *Polyhedron* **2003**, *22*, 2027–2038. (b) Kitagawa, Y.; Shoji, M.; Koizumi, K.; Kawakami, T.; Okumura, M.; Yamaguchi, K. *Polyhedron* **2007**, *26*, 2154–2160.

(18) (a) Miyazaki, Y.; Wang, Q.; Sato, A.; Saito, K.; Yamamoto, M.; Kitagawa, H.; Mitani, T.; Sorai, M. *J. Phys. Chem. B* **2002**, *106*, 197–202. (b) Ikeuchi, S. Doctoral Thesis, Osaka University, Japan, 2005. (c) Ikeuchi, S.; Saito, K.; Nakazawa, Y.; Mitsumi, M.; Toriumi, K.; Sorai, M. *J. Phys. Chem. B* **2004**, *108*, 387–392.(d) Ikeuchi, S.; Saito, K.; Nakazawa, Y.; Sato, A.; Mitsumi, M.; Toriumi, K.; Sorai, M. *Phys. Rev. B* **2002**, *66*, 115110 (7 pages). (e) Saito, K.; Ikeuchi, S.; Nakazawa, Y.; Sato, A.; Mitsumi, M.; Yamashita, T.; Toriumi, K.; Sorai, M. *J. Phys. Chem. B* **2005**, *109*, 2956–2961. (f) Ikeuchi, S.; Yamamura, Y.; Mitsumi, M.; Toriumi, K.; Saitoh, H.; Atake, T.; Saito, K. *Chem. Lett.* **2009**, *38*, 1190–1191.(g) Ikeuchi, S.; Yamamura, Y.; Yoshida, Y.; Mitsumi, M.; Toriumi, K.; Saito, K. *J. Phys. Soc. Jpn.* **2009**, *78*, 094704 (6 pages). (h) Ikeuchi, S.; Yamamura, Y.; Yoshida, Y.; Mitsumi, M.; Toriumi, K.; Saito, K. *Bull. Chem. Soc. Jpn.* **2010**, *83*, 261–266.

(19) Perrin, D. D.; Armarego, W. L. F. *Purification of Laboratory Chemicals*; Pergamon Press: New York, 1988.

(20) Hartke, K.; Rettberg, N.; Dutta, D.; Gerber, H. -D. *Liebigs Ann. Chem.* **1993**, 1081–1089.

(21) (a) Altomare, A.; Burla, M. C.; Camalli, M.; Cascarano, G. L.; Giacovazzo, C.; Guagliardi, A.; Moliterni, A. G. G.; Polidori, G.; Spagna, R. *SIR97. J. Appl. Crystallogr.* **1999**, *32*, 115–119.(b) Sheldrick, G. M. *SHELXL-97*, Program for Crystal Structure Determination; University of Göttingen: Göttingen, Germany, 1997. (c) Wakita, K. *Yadokari-XG*, Software for Crystal Structure Analyses; 2001; Release of Software (Yadokari-XG 2009) for Crystal Structure Analyses, Kabuto, C.; Akine, S.; Nemoto, T.; Kwon, E. *J. Crystallogr. Soc. Jpn.* **2009**, *51*, 218–224.

(22) Kawamura, T.; Ogawa, T.; Yamabe, T.; Masuda, H.; Taga, T. *Inorg. Chem.* **1987**, *26*, 3547–3550.

(23) Guijarro, A.; Castillo, O.; Calzolari, A.; J. Sanz Miguel, P.; J. Gomez-Garcia, C.; di Felice, R.; Zamora, F. *Inorg. Chem.* **2008**, *47*, 9736–9738.

(24) Stiegman, A. E.; Rice, S. F.; Gray, H. B.; Miskowski, V. M. *Inorg. Chem.* **1987**, *26*, 1112–1116.

(25) Guijarro, A.; Castillo, O.; Welte, L.; Calzolari, A.; Sanz Miguel, P. J.; Gómez-García, C. J.; Olea, D.; di Felice, R.; Gómez-Herrero, J.; Zamora, F. *Adv. Funct. Mater.* **2010**, *20*, 1451–1457.

(26) We proposed from X-ray diffuse scattering, lattice parameters, atomic displacement parameter, and polarized Raman spectra that the valence-ordering state of $[Pt_2(EtCS_2)_4I]_\infty$ in the metallic regime appears to be a dynamic two-dimensional CDW state in which the valence states of Pt^{2+}—Pt^{2+} and Pt^{3+}-Pt^{3+} are replaced with the vibration of an iodide ion.[11] The validity of this model has been confirmed by the experiments composed of diffuse X-ray scattering and resonant X-ray scattering.[15a]

(27) (a) Kwak, J. F.; Beni, G.; Chaikin, P. M. *Phys. Rev. B* **1976**, *13*, 641–646. (b) Chaikin, P. M.; Greene, R. L.; Etemad, S.; Engler, E. *Phys. Rev. B* **1976**, *13*, 1627–1632.(c) Chaikin, P. M. In *The Physics and Chemistry of Low Dimensional Solids*; Alcácer, L., Ed.; NATO ASI Ser.; D. Reidel Publishing: Dordrecht, The Netherlands, 1980; pp 53−75.

(28) Tanaka, H.; Kuroda, S.; Yamashita, T.; Mitsumi, M.; Toriumi, K. *Phys. Rev. B* **2006**, *73*, 245102 (12 pages).